1

Introduction

Escribir, por ejemplo: "La noche está estrellada,
y tiritan, azules, los astros, a lo lejos."
Pablo Neruda (Veinte poemas de amor y una canción desesperada)

1.1 Exoplanets

DURING the last decade, we have witnessed the birth of a new branch of astronomy: the study of planets orbiting stars other than the Sun. Three years after the discovery of the first planets around pulsars (Wolszczan & Frail 1992), Mayor & Queloz (1995) announced the first exoplanet orbiting around a Sun-like star, 51 Peg. This first scientific demonstration that the Sun is not the only star which is accompanied by planets, also raised important questions that had no answer with prevailing theories of planet formation: How can a planet be orbiting a pulsar? How can a Jupiter-like planet be orbiting as close to the parent star as to give one whole turn every ∼4.5 days? These surprising first results were just the beginning of a whole set of questions that arose almost at the same cadence as planets were detected. One important consequence of these questions was the necessity to find more systems, in order to try to distinguish between regularity and peculiarity in these exo-worlds. As a consequence, and as the refinement of the techniques evolved, more and more planets have been detected, providing clues to the planetary formation in other stellar systems.

Most of the 157 [1] (at the moment of writing these lines) known planets have

[1] as considered by the Extra-solar Planets Encyclopaedia, by J. Schneider: http://www.obspm.fr/encycl/encycl.html

been detected using the same technique, based on the precise radial velocity measurements of the host star. In this Section, we briefly review this and other techniques used to detect exoplanets, paying special attention to their major findings and the current status. After that (Section 1.2), we will concentrate on the transit method, providing the planetary parameters that can be known and reviewing the estimations of the detection rates for transit searches. The first planet that exhibited transits, which is also currently the best-known planet outside our Solar System, is treated in more detail in Section 1.3. This object, according to some authors, turned out to be bigger in size than expected, and several interesting discussions arose from this fact. These are summarized in Section 1.4. A technique that can serve as a diagnostic for exoplanetary atmospheres is described in Section 1.5, and finally we outline the current theories for the formation of these objects (Section 1.6).

1.1.1 Working definitions

Extrasolar planet: We will use in this work the Working Group on Extrasolar Planets (WGESP) of the International Astronomical Union (IAU) definition of a **planet**[2], which states:

1. Objects with true masses below the limiting mass for thermonuclear fusion of deuterium (currently calculated to be 13 Jupiter masses for objects of solar metallicity) that orbit stars or stellar remnants are"*planets*" (no matter how they formed). The minimum mass/size required for an extrasolar object to be considered a planet should be the same as that used in our Solar System.

2. Substellar objects with true masses above the limiting mass for thermonuclear fusion of deuterium are "brown dwarfs", no matter how they formed nor where they are located.

3. Free-floating objects in young star clusters with masses below the limiting mass for thermonuclear fusion of deuterium are not "planets", but are "sub-brown dwarfs" (or whatever name is most appropriate).

As pointed out by this group, this constitutes a reasonable working definition of a *planet*, which is a compromise between definitions based on the deuterium-burning mass and the formation mechanism. A better definition will have to wait until more knowledge is acquired.

[2]http://www.ciw.edu/boss/IAU/div3/wgesp/definition.html

We will use the term *exoplanet* as a synonym of the previous concept, as it is also widely used in the community.

Hot Jupiter: The term "Hot Jupiter" will be used throughout this work to mean the planets with masses $M_P \sin i \leq 13\ M_{Jup}$ orbiting close to a parent solar-like star (a < 0.1 AU). They are also referred to in the literature as "*51-Peg like objects*" or "*close-in extrasolar giant planets (CEGP)*". Some authors (e.g. Bouchy et al. 2004) have suggested the term "*Very Hot Jupiter*" or "*extremely close-in extrasolar giant planet*" for the planets with periods much lower than 3 days (implying typically orbits with a < 0.025 AU). As there is no clear consensus in the division among these two classifications, we will adopt the more general "Hot Jupiter" denomination as defined above, but we emphasize that it constitutes a *working definition* throughout this work.

1.1.2 Exoplanets around pulsars

Pulsars are the cores that remain after a Supernova explosion of a star with a mass between 15 and 30 $M_\odot$. These cores are neutron stars, which host strong magnetic fields. If the spin axis of the star and its magnetic field are not aligned, then a beam of radio waves hits the Earth at extremely regular intervals, which range between 2 milliseconds and 2 seconds. The typical rate of change of the period of these objects is thought to be one second every ten million years (van Straten et al. 2001). Thus, changes in the period faster than this are the effect of orbiting companions to the pulsar. The precision in the pulsar timing is such as to detect objects with Earth masses or even lower. For a detailed review of these concepts and pulsar astronomy in general, we recommend the book by Lorimer & Kramer (2005).

The first indirect detection of an exoplanet was made by Wolszczan & Frail (1992), and in later works (Wolszczan 1994, Wolszczan 2000) the model was refined, in order to establish the existence of one Mercury-sized planet (A), two Earth-sized planets (B and C), and an asteroid-mass object (D, Wolszczan & Konacki 2005), with masses of 0.020, 4.3 and 3.9 $M_\oplus$, and 0.15 M_{Pluto} orbiting at distances of 0.19, 0.36, 0.46 and 2.7 AU respectively from the 6.2-millisecond pulsar PSR B1257+12.

The pulsar planets have also provided the first demonstration of orbital resonances between exoplanets (Wolszczan 1994; Konacki, Maciejewski, & Wolszczan 1999), as planets B and C exhibit a near 3:2 mean motion resonance. The gravitational perturbations between the two planets have been detected by the same authors, and used to estimate the masses and inclinations of the orbits of the two most massive planets (Konacki & Wolszczan 2003b). The almost coplanar measured inclinations, and the near 3:2 resonance, strongly

support the hypothesis of a disk origin for these planetary system.

It is currently thought that these objects formed in a massive circum-pulsar disk, instead of being remains of an original planetary system of the pulsar parent star that survived the Supernova explosion. Miller & Hamilton (2001) and Hansen (2002) examined the conditions of survival and evolution of these pulsar protoplanetary disks, concluding that these planets should grow in a typical $\sim 10^7$ yr timescale, if the initial disk is sufficiently massive (greater than 10^{28} g). A smaller disk would not survive the evaporation caused by the pulsar accretion flux. There are some proposed schemes for the quick formation of such a massive disk, for instance by tidal disruption of a stellar companion (Stevens, Rees, & Podsiadlowski 1992; Phinney & Hansen 1993) or in the process of a white dwarf merger (Podsiadlowski, Pringle, & Rees 1991; Livio, Pringle, & Saffer 1992). These processes would not be very common. That would explain the lack of planetary companions in the vast majority of millisecond pulsars (48 Galactic pulsars studied by Lorimer, 2001).

1.1.3 The Radial Velocity Searches

The precise study of the radial velocity behavior of nearby dwarf stars has been the most successful method to detect exoplanets to date. Since the first detection of a companion to 51 Peg (Mayor & Queloz 1995), most of the 157 known planets (as of May 2005) have been found as a result of velocity perturbations in the host star induced by the presence of a planetary mass companion. The companion pushes the star back and forth along our line of sight at a velocity with an amplitude of K_s; if we assume that $\mathrm{M}_p \ll \mathrm{M}_s$, and the eccentricity of the planet's orbit is e, then the minimum mass of the planet is given by the expression:

$$M_p \sin i \simeq \left(\frac{P}{2\pi G}\right)^{1/3} K_s M_s^{2/3} (1-e^2)^{1/2} \tag{1.1}$$

and, from the Kepler's laws:

$$a_p \simeq \left(\frac{G M_s}{4\pi^2}\right)^{1/3} P^{2/3} \tag{1.2}$$

where M_p is the mass of the planet, a_p is the orbital semimajor axis, M_s is the mass of the star and i is the orbital inclination (see Figure 1.1). Using various identities leads to an expression for the amplitude of the movement in the form:

$$K(m/s) = \frac{30 M_p \sin i}{(a_p M_s)^{1/2}} \tag{1.3}$$

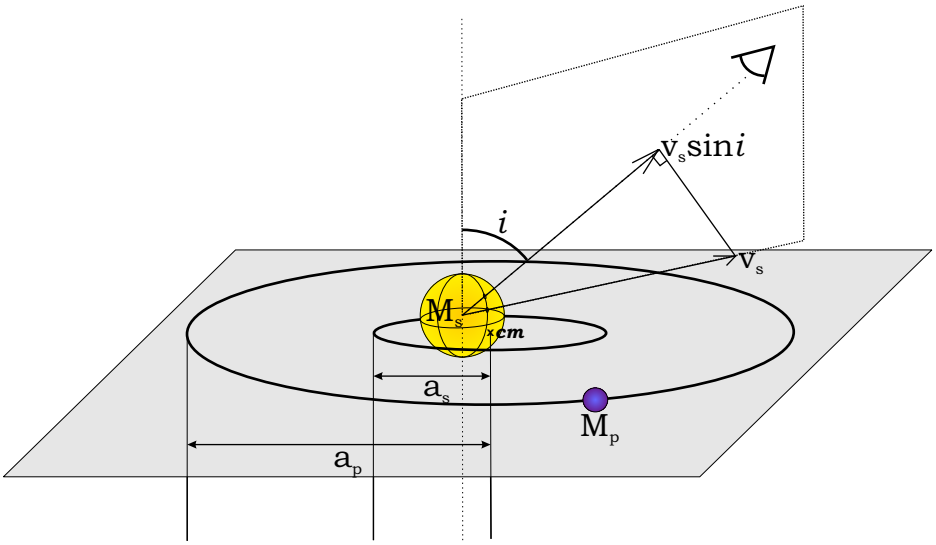

FIGURE 1.1— Schematic view of the main orbital definitions. The star s and the planet p orbit their center of mass cm, in circular orbits with a radius of a_s and a_p respectively. The orbital plane is plotted in gray, and the inclination of the orbit i is defined as the angle between the normal to this plane and the observer's line of sight. The observer is located in the upper right part of the diagram. An edge-on orbit corresponds to an angle of 90°. The reflex motion of the star v_s, when measured along the line of sight, is affected by the sine of this angle.

where the M_p is given in Jupiter masses, M_s in Solar masses and a_p in AU. This movement of the star can be accurately measured using the Doppler effect. The shift produced by a planetary object is of the order of tens or hundreds of m/s (the amplitude of the Sun's movement due to Jupiter is ∼12.5 m/s, due to Saturn ∼4 m/s, and due to the Earth ∼8 cm/s; 51 Peg b moves the host star by 59 m/s), which translates to the necessity to measure shifts in the spectral lines with a precision of roughly 1/1000 of the spectral line width. To achieve this, the radial velocity surveys[3] observe typically sun-like stars (because many spectral lines are needed to improve the measurements) and slow rotators (because fast rotation causes the lines to be broader, and thus the precision is decreased). The information on the radial velocity of the star contained in all spectral lines needs to be concentrated to achieve the required precisions. This is done by computing the cross-correlation between each observed spectrum and a reference spectrum.

[3] see, for instance, *http://www.obspm.fr/encycl/searches.html*

This reference may be the spectrum of a standard star with well-established radial velocity, or one spectrum of the program star itself. The technique of the cross-correlation function was firstly applied to astronomy by Simkin (1974).

The spectrograph behavior has also to be kept under control, to achieve the required precisions, and a radial-velocity reference serves to accomplish this. There are currently two different techniques to establish this reference: a simultaneous thorium-argon lamp observation (see, e.g., Konacki et al. 2003c) and an Iodine absorption cell (see, e.g., Cumming, Marcy, & Butler 1999 and references therein). While the Iodine cell is placed into the path of the star signal, before entering the spectrograph (and thus reducing the signal of the star), the thorium lamp is observed simultaneously as the object (with optical fibers) and thus fainter objects can be measured with the required precision to detect planetary mass objects. It is estimated that the Th-Ar technique is 6 times more efficient than the Iodine absorption cell (e.g., Udry, S. 2004, communication at the XVI Canary Islands Winter School).

Another difficulty with the radial velocity technique is the necessity to maintain good tracking on the star, as its slight movements in and out of the slit can produce spurious radial variations of the star.

State-of-the-art instruments, such as HARPS (Pepe et al. 2002), working at the 3.6 m ESO telescope at La Silla Observatory (Chile), are beginning to obtain precisions of 0.4 m/s. These allow the detection of objects with roughly Neptune's size or even smaller ones (Santos et al. 2004b; McArthur et al. 2004; Butler et al. 2004).

Despite the unquestionable success of this technique in the last decade, there are a few drawbacks. Below 1 m/s, the precision in the radial velocities is not longer determined by the instrument, but by the intrinsic atmospheric pulsations of the star (asteroseismology), which can have amplitudes of several m/s (Mayor et al. 2003), and by the magnetic features on the atmosphere, such as spots, faculae and flares. Even if some of these effects can be modelled and removed (Saar et al. 2003, Kürster et al. 2003), the difficulty increases when trying to reach lower detection thresholds. Thus, it seems difficult for this technique to reach the detection threshold of Earth-sized exoplanets.

Another mayor drawback of the radial velocity searches is that the orbital inclination cannot be known, and thus the exact mass of the planet remains unknown. Actually, only lower limits on the mass can be provided. There are at least two ways to solve the inclination degeneration: astrometric measurements (need to be taken from space to achieve the required precisions) with just one successful case: GJ 876 (Benedict et al. 2002), and the transit method, which will be discussed deeply in this work.

1.1.4 Characteristics of the known exoplanets, derived from the radial velocity surveys

From the sample of 157 planets detected around 138 stars, using mainly the radial velocity technique, a few trends and characteristics of the objects found so far and their host stars are worth mentioning:

- The **fraction of stars** whose planets have masses $M_p > 0.47 M_J$, determined from the Elodie survey (S. Udry, communication at the XVI Canary Islands Winter School) is:

  0.7±0.5% of the surveyed stars have planets with periods below 5 d,

  4.0±1.1% with periods below 1500 d (4.1 y) and

  7.3±1.5% with periods below 3900 d (10.7 y).

- The **secondary mass function** is increasing towards low-massive planets, while it also increases toward stellar companions with masses $\gtrsim$0.1 $M_\odot$ (see, e.g. Halbwachs et al. 2003). There is a noticeable lack of brown dwarf companions orbiting close to their host star, which is commonly referred as the "brown dwarf desert". This might point towards a different formation mechanism for the stellar and the planetary companions.

- The **eccentricities** of most of the planets with semimajor axis above 0.06 AU are distributed almost uniformly between 0 and 0.7. All planets with lower semimajor axis reside in circular orbits (see Goldreich & Soter 1966 for an estimation of the circularization timescales). The origin of the eccentricities for single planets is not well understood (see Marcy et al. 2003 and references therein for plausible mechanisms).

- The **stellar metallicity** of the host stars seems higher for stars with detected planets than for those without detected planets (see for Santos et al. 2003 and Israelian 2003 for reviews on studies on the iron content, and on other metals, respectively). For instance, an homogeneous spectroscopic study of the [Fe/H] for 98 exoplanet host stars revealed that, while only about 3% of the stars in the CORALIE sample were found to be orbited by a planet, this number increased to 25% for stars with [Fe/H] above +0.3 (Santos, Israelian, & Mayor 2004). This might be telling us that the metallicity plays a key role in the formation of giant planets; in particular, there seems to be a need for a high metal content to form massive planets (M>4 M_J, Udry et al. 2002).

- The **period-mass distribution** reveals a lack of massive planets in short period orbits (Udry et al. 2002, Zucher & Mazeh 2002). Furthermore, there seems to be a shortage of planets in the 10-100 d period range, and a lack of light planets ($M_p \sin i$ <0.75 M_J) in orbits with periods larger than ∼100 d (Udry, Mayor, & Santos 2003). These authors provide possible implications in the distribution of these effects, which seem to be in agreement with the current migration scenarios. Another characteristic of this distribution is an apparent "pile-up" of planets with periods in the 3-3.5 d range. Roughly half of the planets with periods below 10 d have periods in this short range, which may also be providing clues for the migration history of these objects (Gaudi, Seager, & Mallén-Ornelas 2005).

1.1.5 Microlensing

Planets orbiting around other stars can also be detected with the gravitational microlensing effect (Mao & Paczyński 1991; Gould & Loeb 1992). When a star (the *lens*) passes in front of a background *source*, this effect causes a magnification with a well known symmetrical light curve profile. If the star is orbited by a planet, it will also leave a signature on the light curve, which can even potentially serve to discover earth-sized planets (Bennett & Rhie 1996). Several projects have followed this approach (MACHO: Alcock et al. 1993, PLANET: see, e.g., Kubas et al. 2005 and references therein, OGLE: Udalski 2003b, MOA: Bond et al. 2001, MPS: Rhie 2001). Bond et al. (2004) claim the first confirmed detection of a planetary microlensing event (Figure 1.2) detected from two different sites (the event was named OGLE 2003-BLG-235/MOA 2003-BLG-53, O235/M53 hereafter). The shape of the event can provide the mass ratio between the star and the planet, and the distance of the planet to the star at the moment of the event. Unfortunately, these events are unique, and almost impossible to be observed repeatedly. Also, the blend between the source and the lens (which is the system star-planet) makes it difficult to measure the characteristics of the star, and thus to determine the planetary mass. In the case of O235/M53, the proper motion of the star (lens) should allow resolving lens and star in about 10 years, if adaptative optics are used (Bond et al. 2004). Only at that time will the assumed main sequence nature of the lens star be proven.

Apparently, the power of this method resides in its ability to detect planets in many different systems (Bennett & Rhie 2002), which include planets in very wide orbits, low mass planets, and even planets in other galaxies. A space mission proposed by these authors, using a 1-2 m aperture space telescope to monitor $\sim 10^8$ Galactic Bulge main sequence stars, should allow the

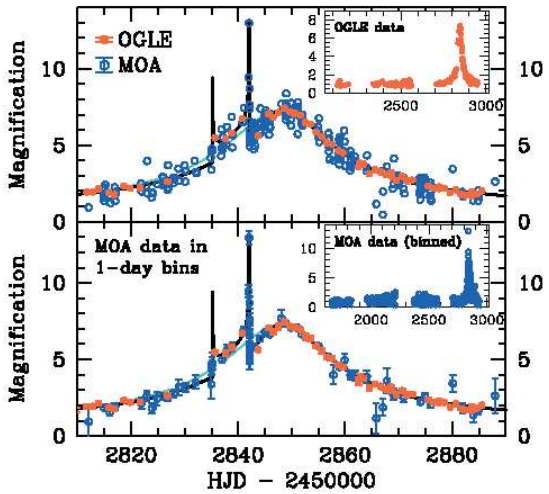

FIGURE 1.2— Light curve with best-fitting and single-lens models of O235/M53 (from Bond et al. 2004).

determination of the average number of planets per star down to 0.1 $M_\oplus$ at separations from ∼0.7 AU to ∞ for terrestrial planets and from 0 AU to ∞ for giant planets, among other scientific outputs.

1.1.6 Direct imaging

Direct observations of exoplanets face the difficulty of the high contrast between the light coming from the star and from the planet, which is of the order of $\sim 10^9$ in the optical and $\sim 10^6$ above ∼10 μm, for a Jupiter-like planet in a Jupiter-like orbit. Coronography and interferometry is planned at the different largest telescopes, both from ground and space (see Lawson, Unwin, & Beichman 2004, table 6, of the NASA TPF Precursor Science document for a review[4]). The most sensitive cases are young big planets orbiting far out from the parent star (d$\gtrsim$50 AU), around nearby stars. These detections, are thus complementary to those of the radial velocity and transit searches, which are more sensitive to planets close to the central star.

A promising candidate for the first detection of a exoplanet with direct imaging techniques is the candidate planetary companion to 2MASS1207334-393254 (hereafter 2M1207, Chauvin et al. 2004). It was detected using the

[4]The file can be retrieved at http://planetquest.jpl.nasa.gov/TPF/tpf_index.html

VLT/NACO adaptative optics system. It is apparently orbiting at a distance of ∼55 AU of the ∼25 M_J brown dwarf 2M1207. Near Infrared photometry (Figure 1.3, left) and spectroscopy are compatible with a spectral type of the companion of L5-L9.5, which places the object in the planetary regime with a mass of M=5±2 M_J, according to different evolutionary models, and a temperature of T_{eff}=1250±200 K (Chauvin et al. 2004). A later study with the HST seems to confirm the planetary nature of this candidate (Schneider et al. 2005, Figure 1.3, right).

New observations with the same optical configuration, taken at three different epochs, show that the candidate shares the same proper motion as the brown dwarf, and thus it is not, with a high confidence level, a stationary background object (Chauvin et al. 2005, accepted).

Another massive planet or minimum mass brown dwarf has been reported recently by the same investigation group, around the young nearby star AB Pic (Chauvin et al. 2005b, accepted). It was detected as a faint, red source located 5.5″ South of the AB Pic star, and apparently it also shares the same proper motion. The evolutionary models predictions, based on the JHK photometry, indicate a mass of 13 to 14 M_J for this object, if its age is ∼30 Myr.

The masses and sizes of these directly detected objects rely on predictions from evolutionary models (such as Burrows et al. 1997, Chabrier et al. 2000, Baraffe et al. 2002), which depend on hard-to-measure estimates of the age of the system. Thus, these mass measurements of the planets do not achieve the precision obtained by the radial velocity surveys.

1.1.7 Astrometry

As in the case of the radial velocity searches, this method relies in the gravitational wobble induced by a planet in its star. If D is the distance to the star (in parsecs) and a is given in AU, then the observed wobble is:

$$r(marcsec) \sim 1000 \frac{M_p a}{M_s D} \tag{1.4}$$

It should be noticed that this technique then favors the detection of massive planets in large orbits around nearby stars. If we were observing our Solar System at a distance of 10 pc, then the wobble induced by Jupiter would have a maximum amplitude of r=500 $\mu arcsec$; Uranus would move the Sun by r=100 $\mu arcsec$, and the Earth only r=0.3 $\mu arcsec$.

In this technique, the movement of the star is measured directly from the center of the stellar profile in one image, and thus needs systems with superb resolving power. This implies the use of interferometry, of space-borne telescopes, or both. For this reason, this technique will provide excellent tests and

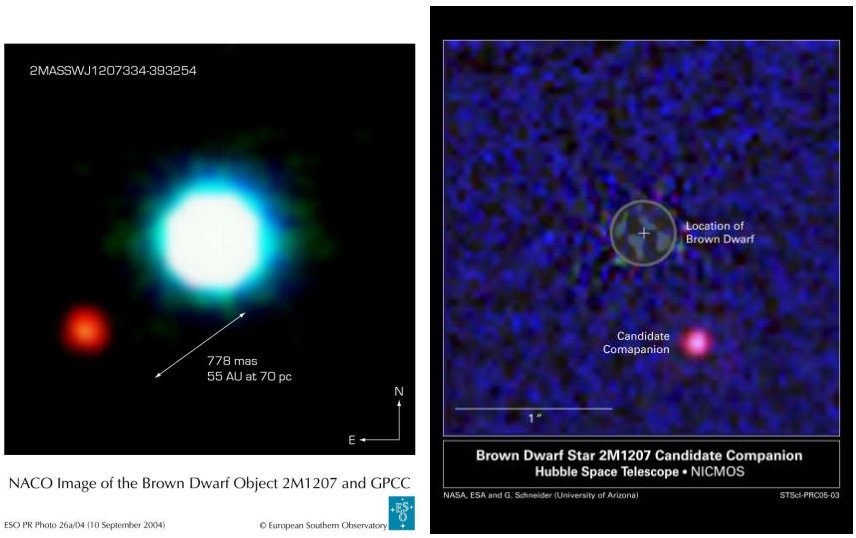

FIGURE 1.3— Left: The possible first exoplanet detected by direct imaging, around the brown dwarf 2M1207, showed in blue (Chauvin et al. 2004). Right: confirmation of the red object with HST data, by Schneider et al. (2005).

technology for the future space interferometric missions, such as Darwin-TPF (see, e.g. Fridlund, Henning, & Lacoste 2003), aimed to take images and spectra of Earth-like planets around nearby stars. But, it seems that it will be very difficult to measure the center of a star with an accuracy better than 1 $\mu arcsec$, because of distortions in the star's image created by stellar spots.

As these lines are written, there has been only one important published success of the astrometric method, when it was used to estimate the inclination of the planet around the M4V star GJ 876 (Benedict et al. 2002). To study the perturbation on the star caused by the most massive planet (1.89 M_J) in the system, GJ 876b, the Fine Guidance Sensors (FGS) on-board HST were used to estimate the amplitude of the astrometric perturbation of the planet as r=250±60$\mu arcsec$. As a direct consequence, and knowing the orbital parameters (P=61 d, a=0.21 AU, e=0.1, minimum mass=1.89 M_J) from radial velocity measurements (Delfosse et al. 1998, Marcy et al. 1998), the orbital inclination of the planetary companion was estimated as 84±6°, which, together with the minimum mass determination, resulted in a measured mass of the object of M_p=1.9±0.5 M_J.

1.2 The transit method

The first reference about the transit method is given in Struve (1952). If a planet with a radius R_p is seen (from a far enough place, such that the perspective effects are negligible) crossing the disk of a star with radius $R_\star$ (causing an event called *transit*), then the flux of the star will decrease by:

$$\Delta F_s = \frac{{R_p}^2}{{R_s}^2} \tag{1.5}$$

In the case of Jupiter passing in front of the Sun, this ΔF_s would be $\sim$1%, that is easily detectable with ground-based photometry. The Earth would produce an $\sim$0.0084% transit, which can be detected with space telescopes (Brown et al. 2001), but is not currently possible from ground. Assuming a circular orbit, the transit would last (Seager & Mallén-Ornelas 2003):

$$t_T = \frac{P}{\pi} \arcsin\left(\frac{R_s}{a \sin i}\left\{[1 + (R_p/R_s)]^2 - [(a/R_s)\cos i]^2\right\}^{1/2}\right) \tag{1.6}$$

where P, a and i are the period, radius and inclination of the planet's orbit. The inclination is the angle between the normal of the orbital plane and the line of sight. This means that $i = 90^\circ$ is for a planet crossing the star through the middle (solid light curve in Figure 1.4 and 1.5). The typical transit durations for Hot Jupiters are 2-3 hours. Assuming circular orbits for the planets, and with a first order approximation M_s=R_s (in Solar units), Figure 1.6 plots the maximum duration of a 1 R_J planetary transit as a function of the mass of the star and the period of the planet. This maximum duration can be used as a tool to discard false positives in transit searches.

For such an effect to be observable, the orbit of the planet must cross the line of sight of the star. The probability for this to happen is:

$$P_{tran} = \arctan\frac{R_s + R_p}{a_p} \sim \frac{R_s + R_p}{a_p} \tag{1.7}$$

which is low for planets such as Jupiter in our Solar System (P_{trans}=0.089%), but can be as high as 10% for the Hot Jupiter class objects. The existence of this kind of objects, orbiting $\sim$0.7% of the main sequence stars in the solar neighborhood (see Section 1.1.4), and the relatively high probability of transits, have motivated a number of transit searches for exoplanets (see Horne et al. 2002, for a review[5]).

[5] A list of the transit searches is available at: http://star-www.st-and.ac.uk/~kdh1/transits/table.html

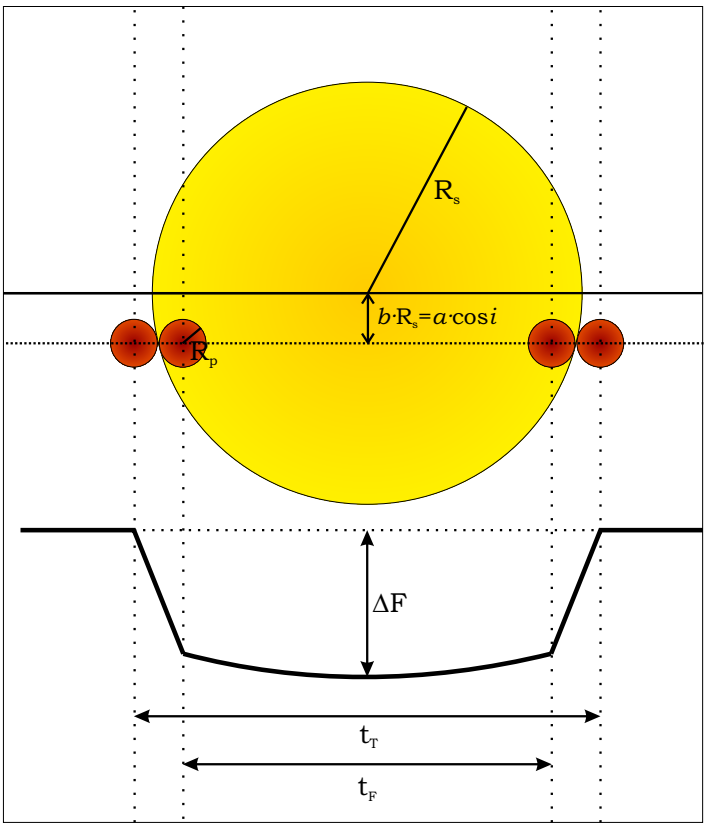

FIGURE 1.4— Schematic view of the main transit definitions. Top: The planet is plotted in four different positions (first to fourth contact). The flux of the star (black solid line) is reduced by an amount ΔF during a transit with a total duration of t_T; the duration between ingress and egress is t_F, and it is also referred as the "flat part" of the transit. The slight curvature of this part is a consequence of the star's limb darkening. Also plotted is the impact parameter b, where the definition of the inclination angle i is represented in Figure 1.1.

The first transiting planet, HD 209458b, was discovered in 2000 (Charbonneau et al. 2000, Henry et al. 2000), but it had been previously detected with the radial velocity method (Mazeh et al. 2000). We will treat this object in detail in Section 1.3.

The success of these transit searches (discovering planets with the transit method, not previously known from any other technique) came from the OGLE-III team (Udalski et al. 2002, 2002b, 2002c, 2003, 2004), who have at this time

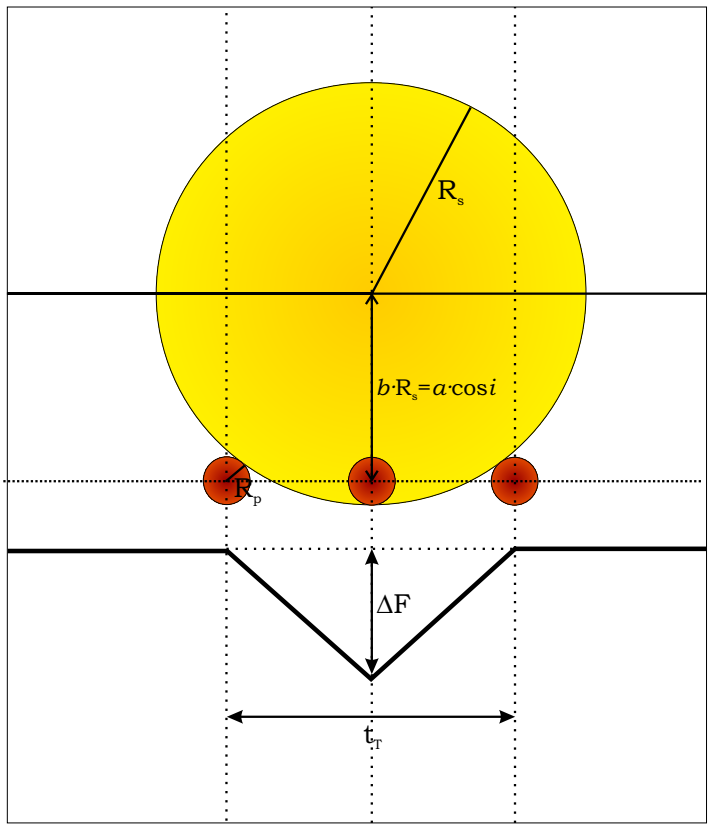

FIGURE 1.5— Same as Figure 1.4, for the case in which the planet is never projected completely on the stellar disk is plotted in the bottom part. In this case, there are no second nor third contacts, an thus there is no "flat part" of the transit (i.e., $t_F = 0$).

published a list of 177 transiting planet candidates. This project uses a 1.3 m telescope placed at the Observatorio de La Silla in Chile, to monitor dense fields for long period of times, with I magnitudes ranging from 13.5 to 17. This places the bulk of the stars at typical distances of ∼1000 pc. Further follow-up works demonstrated that the vast majority of these candidates turned out to be false positives, but 5 planets have been detected to date (OGLE-TR-56b: Konacki et al. 2003a, OGLE-TR-113b and OGLE-TR-132b: Bouchy et al. 2004, independent confirmation of OGLE-TR-113b: Konacki et al. 2004, OGLE-TR-111b: Pont et al. 2004, OGLE-TR-10b: Konacki et al. 2005). Three of these planets, (OGLE-TR-56b, OGLE-TR-113b, OGLE-TR-132b),

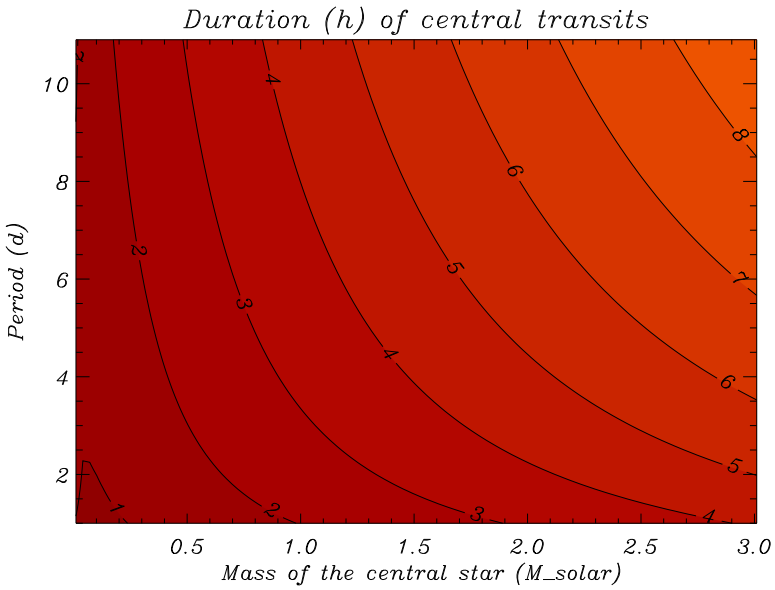

FIGURE 1.6— Maximum duration (in hours) of a central (i=90°) transit, as a function of the star's mass (in Solar units) and the planet's period (in days). Circular orbits and $M_\star$=$R_\star$ (main sequence stars) have been assumed.

apparently orbit their stars with shorter periods than had ever been observed with the radial velocity surveys. This fact led to several authors to group these objects under the terminology of "Extremely Hot Jupiters". As can be seen in Equation 1.7, the probability of observing transits from Earth is bigger as the planet is closer to its host star.

The advantages of these deep-field transit searches are that the population of main sequence stars is constituted of smaller stars on average, which can lead to the discovery of smaller planets. Also, differential atmospheric extinction problems are less important as the field of view gets narrower. The major drawbacks are the difficulty of the follow-up observations and thus the precision with which the planet's parameters can be known. The kind of studies performed in HD 209458 (discussed in next Section) are difficult, if not impossible, to repeat in these much fainter stars.

1.2.1 The measurable parameters

From the shape and period of the photometric transit (depth of the transit ΔF, total duration t_T, duration of the flat part of the transit t_F, period P), four measurable parameters can be calculated (Seager & Mallén-Ornelas 2003):

The planet to star radius ratio:

$$\frac{R_p}{R_s} = \sqrt{\Delta F} \tag{1.8}$$

The impact parameter b:

$$b \equiv \frac{a}{R_s}\cos i = \Big\{\frac{(1-\sqrt{\Delta F})^2 - [\sin^2(t_F\pi/P)/\sin^2(t_T\pi/P)](1+\sqrt{\Delta F})^2}{1-[\sin^2(t_F\pi/P)/\sin^2(t_T\pi/P)]}\Big\}^{1/2} \tag{1.9}$$

The ratio $a/R_\star$:

$$\frac{a}{R_s} = \Big\{\frac{(1+\sqrt{\Delta F})^2 - b^2[1-\sin^2(t_T\pi/P)]}{\sin^2(t_T\pi/P)}\Big\}^{1/2} \tag{1.10}$$

And the stellar density, assuming $M_p \ll M_\star$:

$$\rho_s \equiv \frac{M_s}{R_s^3} = \Big(\frac{4\pi^2}{P^2G}\Big)\Big(\frac{a}{R_s}\Big)^3 = \Big(\frac{4\pi^2}{P^2G}\Big)\Big\{\frac{(1+\sqrt{\Delta F})^2 - b^2[1-\sin^2(t_T\pi/P)]}{\sin^2(t_T\pi/P)}\Big\}^{3/2} \tag{1.11}$$

In these formulas limb darkening has not been considered and circular orbits have been assumed. Combining the measured inclination i (which can be extracted from Equations 1.9 and 1.10), with information on the orbit that results from radial velocity measurements (Equation 1.3), it is possible to solve the degeneracy between the mass and the inclination, and get the exact mass of the planet. Assuming a radius for the star (for instance, from the spectroscopic information and the values tabulated in Cox, 2000), and using Equation 1.8, the radius of the planet can be measured. Combining these two physical quantities, it is possible to measure the mean density of the planet.

1.2.2 Expected detection rates

How many stars do we need to survey to achieve significative chances to detect a transiting planet? How many *false positives* (stellar systems) do we expect to identify in such a survey?, and how can we identify them? The answer to this last question will be treated in detail in Chapter 3, while the other two questions are the subject of a work by Brown (2003). In that work, the possible

stellar systems that could produce signals resembling those of transiting planets were categorized in a tree structure, which was defined by the answers to the questions:

- Is the primary of the eclipsing system a main-sequence star (M) or a giant (G)?
- Is the secondary a main-sequence star (S) or a Jovian planet (P)?
- Is the light from the binary undiluted by a third star (U) or diluted (D)?
- If diluted, is the third star a foreground object (F), or is the system a bound triple (T)?

The main configurations that could produce signals similar to the ones produced by a transiting planet are five: MPU (the target of a survey: transiting planets), MSU (grazing transits in systems of two main-sequence stars), MSDF and MSDT (eclipsing systems whose depths are diluted by a third star), and GSU (transits of giants by main sequence stars).

Probability densities for each of these cases were calculated by Brown (2003), under a set of reasonable assumptions and simplifications that could modify the final expected detections by factors of a few. For instance, the luminosity of the secondary component in an eclipsing system was neglected, and circular orbits were assumed. The first of these assumptions might affect the results when compared to the surveys, as the detection of a secondary eclipse in the data is a useful tool to identify a false positive (see Chapter 3).

Integrating the estimated probability densities over all stellar types, over periods in the range 1 d$\leq$P$\leq$30 d, over relative depths 0.01$\leq \delta \leq$0.05, and over transit durations 0.06 d$\leq d \leq$0.25 d, assuming a confusion radius of 20″, and a limiting R magnitude of 12, Brown gets the results summarized in Table 1.1, which prints the expected detection rates per 10^4 surveyed stars. Detections of at least 3, 2, or 0 transits are printed in that table (0 detections would mean that there are eclipses of that category in the surveyed stars, but they were not observed, i.e. the total number of stars in that category), assuming a single-site typical observing campaign (one STARE run on a field of Cygnus, with 211 h of observation on 38 individual nights, spread over an interval of 91 days). All the calculations were made assuming the observed field was in the Galactic plane. Two consequences of these estimations are the need to improve the duty cycle in transit searches (such as combining data from several telescopes located at different longitudes), and to establish rejection tests that help to identify the false positives (Chapter 3 of this work is devoted to this objective). These are

TABLE 1.1— Expected detection rates for a survey such as STARE per 10^4 stars. From Brown (2003).

Category	n≥0	n≥2	n≥3
MPU	1.43	0.74	0.39
MSU	4.56	2.92	2.27
MSDF	1.90	1.52	1.26
MSDT	1.64	1.20	0.98
GSU	0.00	0.00	0.00

expected to be more numerous than real transiting planet detections, a result that is strongly supported by transit surveys up to date (for instance, the case of the OGLE survey discussed before, or our own work discussed later).

1.3 HD 209458b

Currently, the best-known and best-studied exoplanet is orbiting around the G0V star HD 209458. In this section we describe several studies carried out on this planet, which constitute a benchmark in the field.

The planet was discovered (Mazeh et al. 2000) with the radial velocity technique. The spectra were taken using both the HIRES (Vogt et al. 1994) and ELODIE (Baranne et al. 1996) spectrographs, and completed with spectra from CORALIE (Queloz et al. 2000).

In September 1999, the STARE telescope was used to monitor the first transits of an exoplanet around its star (Charbonneau et al. 2000; Figure 1.7). An independent ingress was observed by Henry et al. (2000).

At that moment, there were only 11 known exoplanets, all of them detected with the radial velocity method (apart from the pulsar planets described in Section 1.1.2). There was also some skepticism from diverse authors, like the observations by Gray (1997) apparently showing distortions in the spectral line bisectors; if confirmed, these would argue against the planetary origin of the radial velocities observed in these stars. These observations could not be reproduced (Gray 1998, Brown et al. 1998), and a definite demonstration of the existence of these exoplanets to the more skeptical community came with the detection of transits in HD 209458. These allowed a determination of the planetary radius.

Combining the data with the radial velocity observations, which give $M_p \sin i$, the mass was measured, and thus the mean planetary density (0.38 g/cm^3 in the work of Charbonneau et al. 2000; refined to 0.35 in Brown et al. 2001). This measurement confirmed the suspected gaseous nature of these objects. Several

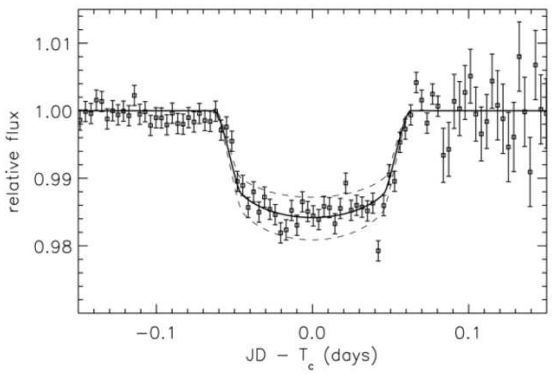

FIGURE 1.7— Transit of HD 209458b observed with the STARE telescope, in September 1999. The curvature at the bottom of the transit is a consequence of the star's limb darkenning. Points are 5 min bins, and the error bars are the standard deviations of the mean in each bin. From Charbonneau et al. (2000).

ground-based multi-color observations were conducted to improve the stellar and planetary parameters, and to measure the limb darkening coefficients, for the first time in a star other than the Sun (Jha et al. 2000, Deeg, Garrido, & Claret 2001).

The best quality light curve was obtained using the spectrograph STIS on board the HST telescope (Brown et al. 2001; Figure 1.8). Attaining an unprecedented precision of $1.1{\cdot}10^{-4}$ per sample point, enough to identify a transit of an Earth-sized object, they improved the parameters of HD 209458b: $R_p = 1.347 \pm 0.060\ R_J$, an orbital inclination of $i = 86°.6 \pm 0°.14$, and a stellar radius of $R_s = 1.146 \pm 0.050\ R_\odot$. The residuals of the fit were used to search for satellites and rings around the planet. Upper limits on the mass and sizes of potential satellites were established in 3 $M_\oplus$ and 1.2 $R_\oplus$, respectively. The presence of large opaque rings was also constrained, to a lesser degree, establishing a maximum size for this structures (if present) of 1.8 radii of the planet.

The spectral information contained in these data set was used by Charbonneau et al. (2002) to detect for the first time an exoplanet's atmosphere. The technique used was transit spectroscopy (described later in this Introduction), whose basic idea consists of measuring the wavelength dependence of the radius of the exoplanet. This dependence is caused by different opacities of the atmosphere components. In a region close to the Na D lines at 589.3

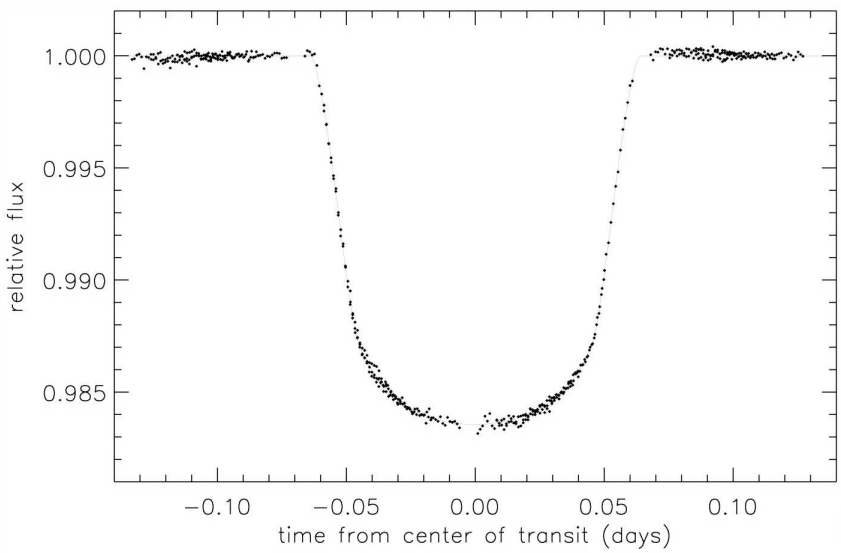

FIGURE 1.8— HST observations of transits of HD 209458 b. The precision per sample point achieved is $1.1{\cdot}10^{-4}$. From Brown et al. (2001).

nm, they compared the ratio of the star's spectrum outside of transit to the spectra when the planet is crossing the disk. Thus, in relative flux, the transit was 0.00023±0.00006 deeper in the region where the sodium absorption was expected. The strength of the sodium absorption was ∼3 times weaker than that predicted by a fiducial model, which assumed solar sodium abundance for the star. The authors interpret this discrepancy in the measured sodium absorption as a consequence of a high cloud deck, a low atomic sodium abundance, or a combination of both effects. Also, the effect of the strong UV bombardment on the planet might play an important role, with possible formation of photochemical hazes.

Later on, Vidal-Madjar et al. (2003) used STIS on board HST to observe the Lyman-α emission line of the star. When the planet was transiting, the emission was reduced by a 15±4% (1σ), which according to these authors is a proof for an extended upper atmosphere on HD 209458b. The implied radius of the planet at these wavelengths is 4.3 R_J. This radius suggests that the upper atmosphere material fills and overflows the Roche lobe (which has a radius of 3.6 R_J. Thus, the atmosphere of this planet is in process of evaporation due to the heavy UV-bombardment of the star at such close distance. They estimate the evaporation

rate as 10^{10} g/s. In a later work (Vidal-Madjar et al. 2004), they used a lower resolution (and wider spectral range) band to search for different species in the planetary upper atmosphere. The detection of absorption in the H I lines at a 5±2% level in this work is consistent to that detected in the previous study, due to the lower resolution in the line. In this second search, they claim the detection of absorption also in the O I (13±4.5%) and C II (7.5±3.5%) lines. Surprisingly, these results would imply that these components are higher in the atmosphere than the less-massive H I, which seems unlikely, and can not be explained if the molecular diffusion dominates at high altitudes, nor if an extreme eddy diffusion transport is able to transport the oxygen and carbon up to the Roche level. To explain the observation, the authors need a mechanism that is able to transport oxygen and carbon up to about the Roche lobe while maintaining their velocity dispersion of at least ∼10 km/s. They propose that the H I is escaping at a high rate, and the hydrodynamical flow of this process drags up the other species, preserving their abundances. This mechanism has been called "blow-off" (Watson, Donahue, & Walker 1981), and it is supposed to keep velocity dispersions for the oxygen and carbon similar or greater than the sound speed (∼10 km/s at 10000 K, which is the estimated upper atmosphere temperature). With these velocity dispersions, the conditions at the upper atmosphere would be such that the whole stellar line would be absorbed by the planetary carbon and oxygen, thus allowing a 10% absorption if they flow up to the Roche lobe.

1.4 On the radii of the transiting planets

One important physical parameter that can be obtained with the transit method is the radius of the planet. Soon after the discovery of 51 Peg (Mayor & Queloz 1995), models for strongly irradiated planets appeared in the literature (Guillot et al. 1996). These models predicted that these short period planets, with effective temperatures above 1000 K, should have their radii significantly larger than Jupiter. The first measurement of an exoplanet's radius came with the discovery of HD 209458b's transits (Charbonneau et al. 2000; Henry et al. 2000). The most precise numbers for its radius are given in the work by Brown et al. (2001), where the high-quality HST photometry allowed to fit independently R_s and R_p. The measured radius in that work was $R_p = 1.347 \pm 0.060$ R_J. A subsequent analysis of the same HST data by Cody & Sasselov (2002), state a value of $R_p = 1.42 \pm 0.10$ R_J. In any case, the published value proved that the planet was a gas giant planet, composed basically of hydrogen. A theoretical study of the radius of HD 209458b by Guillot & Showman (2002), required unrealistically hot temperature of the deep atmosphere of the planet

in order to reproduce the observed radius. Under more realistic temperature conditions, an extra source of energy seemed to be lacking, to make the radius match the observations. These authors proposed one mechanism to account for this extra energy: if a fraction ($\leq$1%) of the incident stellar flux is transformed into kinetic energy at the planet atmosphere, then it could be converted into thermal energy at deeper levels (tens of bars) of the atmosphere, by dynamical processes.

Other studies proposed different extra sources of energy in the planet. Bodenheimer, Lin, & Mardling (2001) also find a difference of $\sim$0.3 R_J between the observed and predicted radius (without an extra source of energy). They suggest (Bodenheimer, Laughlin, & Lin 2003) that the energy arising from ongoing tidal circularization of the planet's orbit could account for such an increased radius. This would require the presence of a yet unseen companion to HD 209458 b, which can still be consistent with the residuals of the radial velocity measurements. In fact, they obtain a good fit to the spectroscopic measurements with an eccentricity of $e \sim 0.03$. This low, but nonzero eccentricity, could explain the increased radius of HD 209458b, if a model without a core for the planet is assumed. For models with a solid core, the eccentricity needed would be of the order of $e \sim 0.1$, which seems inconsistent with the current velocity measurements. A two-body fit of the radial velocity data seems to indicate a possible second companion (companion "c") with a period of $\sim$ 80 days, and mass of $\sim$ 0.12 M_J.

In the study carried by Chabrier et al. (2004), a simple model of one-dimensional irradiation, with incoming flux deposited uniformly over the day side and non-dynamical redistribution of the incident flux because of day-night temperature differences, is found to adequately reproduce the radius of OGLE-TR-56b. But, in order to reproduce the radius of HD 209458b, a significant fraction ($\sim$0.5%) of the incident flux must be transported downward and converted into thermal energy at the radiative-convective boundary. This confirms the results by Showman & Guillot (2002). But it is still necessary to invoke an unknown mechanism able to transport kinetic energy from the top of the atmosphere downwards to the adiabat level, which lies at P$\sim$500 bar for HD 209458b and P$\sim$4000 bar for OGLE-TR-56b (18 and 23 pressure scale heights, respectively). The calculated radii and the measured values are plotted in Figure 1.9. It seems, from these plots, that this mechanism might be taking place in HD 209458b, while for OGLE-TR-56b it is not necessary to invoke any extra source of energy.

Finally, Burrows, Sudarsky, & Hubbard (2003) argue that the radius measured in a transit is systematically larger than the radius that result from the planet evolution codes. This is a consequence of the stellar photons passing

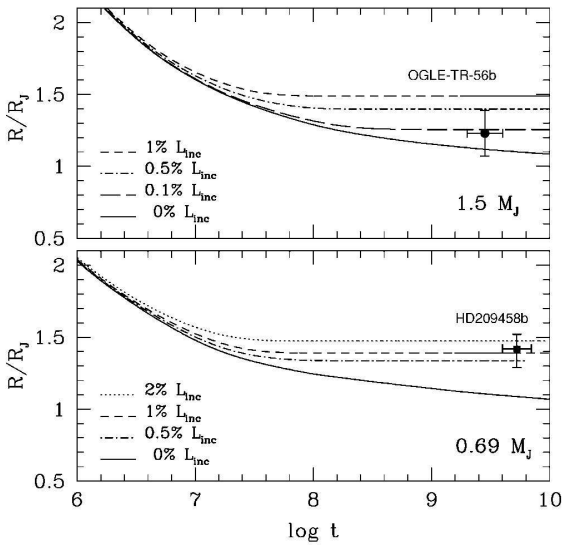

FIGURE 1.9— Evolution of the planetary radii of OGLE-TR-56 b (top) and HD 209458b (bottom), for models without invoking an extra source of energy (solid lines), and assuming conversion of several fractions of the incident luminosity into thermal energy deposited at the adiabatic level. From Chabrier et al. (2004)

obliquely to the limb of the planet. The measured radius of a transit implies an effective optical depth of ~ 1. But the effective optical depth is for a chord that is parallel to the line between the centers of the planet and the star. This can be quite different from the optical depth measured radially from the center of the planet. In fact, there is a significant difference between the pressure level at which the transit beam becomes opaque (1 mbar, according to Fortney et al. 2003), and the one that is calculated for opacity equal to 1 with the models ($\sim$0.1 bar, Baraffe et al. 2003, Figure 5 in that work). Burrows, Sudarsky, & Hubbard (2003) estimated that this effect might add $\sim$0.1 R_J to the estimated radii, and, in the case that the real measurement of the radius of HD 209458b lies in the bottom part of the observational error bar, then no extra source of heating might be necessary to account for the observed radius.

To summarize, there have been three different proposed explanations for the radius of HD 209458b:

- The radius is anomalously large; the transport of a small fraction of the incident flux by kinetic energy (winds) to deep levels of the planet's atmosphere, and the subsequent conversion of this energy into thermal energy

at this level can account for this increased radius. This effect might take place in all the Hot Jupiters, and consequently, all the transiting planets might show strongly inflated radii.

- The radius is anomalously large; this is due to ongoing tidal circularization, which needs the presence of a yet unidentified third body in the system. If this were the case, HD 209458b might be the anomalous case, and the next found transit planets should all show smaller radii.

- The radius is within theoretical expectations, taking into account the factors discussed by Burrows, Sudarsky, & Hubbard (2003). The newfound transiting planets, according to this approach, should all show bigger radii than estimated.

1.5 Transmission spectroscopy

The atmospheres of the transiting planets leave a signature on the observed stellar spectra as they cross the disk. The study of this signature and the extraction of physical information on the atmospheres of these object can be done with a technique called *transmission spectroscopy*. The observations of spectra in transmission are not new for exoplanets; they have been used to study binary stars (e.g. Eaton 1993), and occultations of stars by planets in our solar system (e.g. Smith & Hunten 1990). Several works have aimed to provide clues on what can be observed from the exoplanet's atmospheres with current or near future instrumentation. In this Section, we summarize the two main (and only) works on this subject: Seager & Sasselov (2000) and Brown (2001). We refer the reader to these works for detailed information.

The signal imposed by an exoplanet on the star's spectrum while it is transited is small. As a rough number, the outer parts of the planet that are not opaque to certain wavelengths (i.e. its atmosphere) are not bigger than 10% of the total planetary radius. When superposed on the star's disk, the total area that can act as a probe for the atmosphere is of the order of 10^{-3} to 10^{-4} of the star's area. This signal will be Doppler shifted by a significant amount during a transit of a Hot Jupiter, due to the high orbital velocities of these objects (for the case of HD 209458b, this Doppler shift is about $\pm$ 15 km/s). Out of the several varying sources of radiation that reach the observer from the star/planet system during the transit (namely, thermal radiation from the planet, scattered light from the day-side of the planet, and direct light blocked by the planet), the difference in direct light blocked by the planet at different wavelengths is the best diagnostic for the planet's atmosphere. The thermal contribution and the scattered light effects are at least 10 times smaller than the effect of having

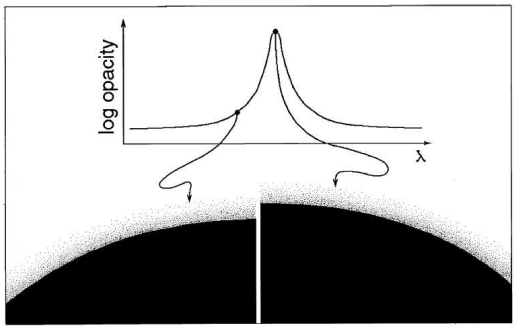

FIGURE 1.10— Atmospheric opacity (shown as a function of wavelength in the upper trace) corresponds directly to apparent radius of the planet, since in opaque regions of the spectrum, one must go to higher altitude and lower density before tangential rays are transmitted. High-opacity regions appear as absorption lines in the spectrum ratio because the planet appears larger at these wavelengths and blocks a larger part of the star's light. From Brown (2001)

material with different opacities at different wavelengths. This dependance of the planet's atmospheric opacity is translated into a variation of the observed planetary radius with wavelength (see Figure 1.10).

The main goal of the works by Seager & Sasselov (2000) and Brown (2001) was to derive theoretical expectations on the variation of the observed planetary radii with wavelength, and to seek the most promising features that might be observable with current instrumentation. To do so, Seager & Sasselov (2000) relied on a self-consistent transmission model based on atmosphere models of Hot Jupiters[6], together with assumptions on the (expected) cloud composition and grain size (10μ grains of $MgSiO_3$, Fe, and Al_2O_3). The cloud base (and cloud top) are fixed in their model once its composition and grain size is determined.

Under a slightly different approach, Brown (2001) cautions that poorly understood physical processes (such as meteorology, photochemistry, cloud processes, etc.) might be important in these objects, and thus constructs a non-self-consistent model, using reasonable assumptions when needed. His model is based on T(P) profiles provided by Sudarsky, Burrows, & Pinto (2000), and solar abundances of H, He, C, N, O, Na, Si and K. The partial pressures of the main molecules (H_2, H_2O, CO, CH_4, N_2 and NH_3) are calculated from the reactive atomic constituents (H, C, N, O), assuming thermodynamic equilibrium

[6]Described in Seager (1999) and Seager, Whitney, & Sasselov (2000), these models provide T(P) profiles, and assume an atmosphere composed of H_2, CO, H_2O and He

at each pressure level. Clouds are supposed to be composed of $MgSiO_3$, with a distribution of grains sizes that peak at 3 μm.

Neither model accounts for stellar photoionization, but Brown (2001) treats the ionization of the alkali metals at high atmospheric altitudes in a schematic way. Helium opacity is included in the model by Seager & Sasselov, but not by Brown. Both authors agree on that the likely extended atmosphere, where this compound is expected to reside, will be highly photoionized, and recombination might populate triplet states of the atom (which are long-lived). The calculation of the population of the low levels of this slow transitions would require a radiative transfer calculation involving not only He, but also H_2 and H, and it would be complicated by the near-horizontal incidence of the ionizing radiation. This led to the non-inclusion of the He opacity in the model by Brown (even if the He is included as a non-reacting component).

As final results of the calculations, both works provide expected transmission spectra for these objects. In order to visualize the dim signals of the planet, Seager & Sasselov (2000) plot the normalized spectra in-transit minus spectra out-of-transit (Figure 1.11). The work by Brown (2001) presents the ratios of spectra in-transit / spectra out-of-transit (Figure 1.12). Both works agree on the fact that the resonance lines of the alkali metals (Na and K) are promising absorption features, together with near infrared molecular absorption bands of CO, H_2O and CH_4. The He triplet line at 1083.0 nm is proposed by Seager & Sasselov (2000) as a "strong" signal, while the work by Brown (2001) doesn't quantify the absorption of this element, for the reasons stated above. Both models agree on the importance and present lack of knowledge of the composition and location of clouds, and the results are strongly dependent on this. The work by Brown (2001) further explores the possibility to measure heavy-element abundances, temperatures, and the vertical temperature structure; although these properties (and the composition and location of the clouds) tend to be somewhat degenerate.

Brown (2001) proposes a cross-correlation of observed spectra to templates from the theoretical models to establish the line strengths of the different elements.

Photoionization in his work apparently reduces the depths of the alkali metals resonance line cores, while there is little or no change in their wings. Altitude-dependent winds would also leave a signature on the spectral lines, but unrealistic values need to be considered for this effect to be detected in the next decades.

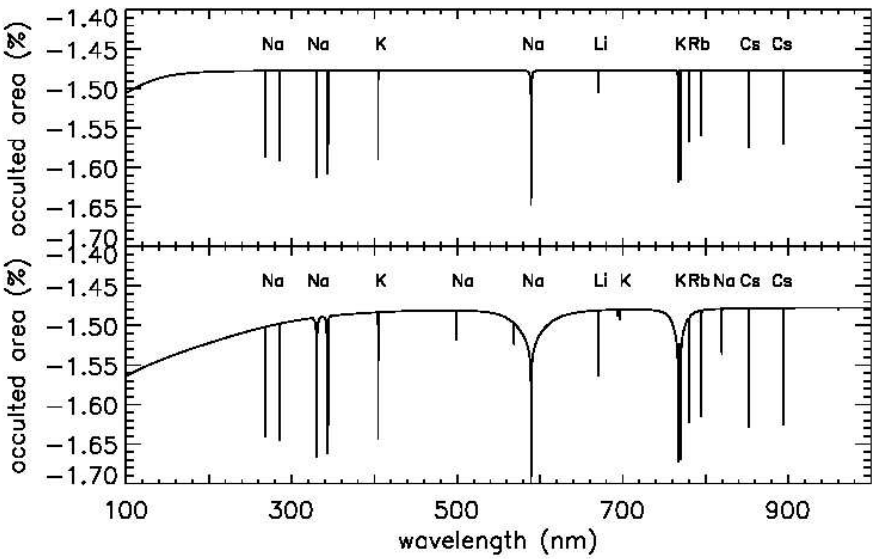

FIGURE 1.11— Upper plot: The normalized in-transit minus out-of-transit spectra, i.e., percent occulted area of the star. In this model the cloud base is at 2.4×10^{-3} bar. Rayleigh scattering is important in the UV. Lower plot: A model with cloud base at 0.2 bar. The stellar flux passes through higher pressures, densities, and temperatures of the planet atmosphere compared to the model in the upper plot. In addition, a larger transparent atmosphere makes the line depth larger. Observations will constrain the cloud depth. From Seager & Sasselov (2000).

1.6 Formation models of giant planets

Observational evidence that the mass function of young objects in star-forming regions extends down to below the deuterium burning limit (Zapatero Osorio et al. 2000) and the absence of good theoretical reasons against it, point towards the same formation mechanism for stars, brown dwarfs and isolated high mass planetary objects (fragmentation during collapse of a molecular cloud). On the other hand, the existence of a "brown dwarf desert" (no objects with masses in the brown dwarf regime orbiting close to a star) in all the radial velocity surveys, and the increasing number of planetary mass objects with smaller masses (see, e.g., Halbwachs et al. 2003) point to a different formation mechanism for orbiting exoplanets than for stars and isolated objects. The fragmentation model is not valid to explain the formation of these objects (Bodenheimer, Hubickyj, & Lissauer 2000). Out of the different formation models that have

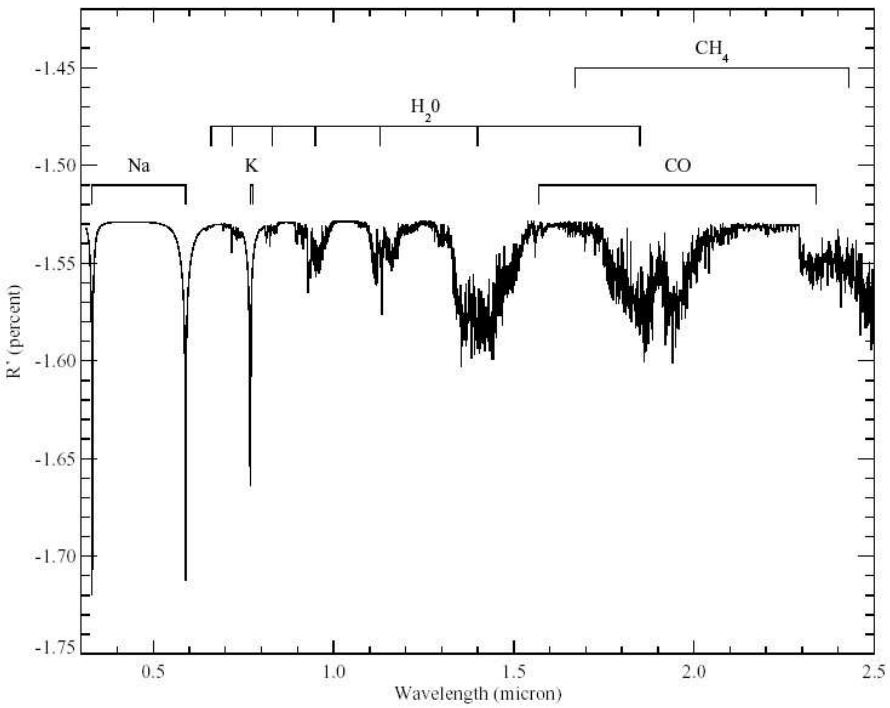

FIGURE 1.12— Fiducial model spectrum ratio vs. wavelength. The maximum value of -1.53 % corresponds to the fraction of the star's light blocked at the wavelengths where the atmospheric opacity is lowest. Over most of the wavelength range, the spectrum was computed at R = 15.000, but it is displayed here averaged and rebinned to R = 3000. Significant atomic and molecular absorption features are labeled. From Brown (2001).

been proposed (see Wuchterl, Guillot, & Lissauer 2000 and references therein for a review), the two hypotheses receiving most attention are the core instability model (or nucleated instability) and the disk instability (or gravitational instability) model.

According to the core instability model (see, e.g., Bodenheimer, & Pollack 1986), the planet is formed in a similar way as a terrestrial planet is, until it reaches a mass that allows to accumulate significant amounts of the surrounding gas in the disk. The gas accretion rate becomes comparable to the planetesimal bombardment when the core reaches a mass of $\sim$10 M_E. At this point, the gas accretion happens very fast, in a phase called runaway accretion. The primary question regarding this scenario is whether planets with small cores can accrete

very massive gaseous envelopes within the lifetimes of gaseous protoplanetary disks (10^6-10^7 y, Strom, Edwards, & Skrutskie 1993, Alencar & Batalha 2002).

In the disk instability model (e.g. Cameron 1978, Boss 1997), the giant planet forms directly from the contraction of a clump formed by gravitational instability in the protoplanetary disk. It seems that this model has never been demonstrated for realistic disk conditions (c.f. Lissauer 2004). Besides, it has difficulties explaining the supersolar abundances of heavy elements in Jupiter and Saturn, and it does not explain the origin of planets like Uranus and Neptune. But the timescales for this process are smaller than those derived from the core instability model (few hundred years).

There is some theoretical controversy associated with the possibility that the planets experience orbital migration, as a consequence of the gravitational torque between the disk and the planet. This torque may allow planets to clear gaps around themselves (Goldreich & Tremaine 1980; Ward 1986; Bate et al. 2003; see Thommes & Lissauer 2005 for a review). Planetary orbits can migrate towards (or, in some circumstances, away from) their parent stars, as a consequence of angular momentum exchange between the planet and the disk. It is thus possible that planets may form at several AU away from their parent star and then migrate inwards to the locations where they are currently observed. This raises several problems, such as the necessity for a stopping mechanism to avoid the planet falling onto the star. We will not get into the details on this and we refer the interested reader to the Thommes & Lissauer (2005) review, and references therein.

1.7 Motivation for the following study

As has been explored in this Introduction, exoplanets that transit their host stars can provide us with valuable physical information, such as a mass measurement (without the degeneracy imposed by the inclination of the orbit in the non-transiting planets), and a radius estimation that is inaccessible by other means. With the occurrence of transits, a new set of follow-up studies becomes possible, as was discussed in Section 1.3. The discovery of transits in the HD 209458 system allowed the development of a series of techniques and studies that served to increase the knowledge on these objects.

However, at the time of beginning this thesis, HD 209458b still remained the only planet to produce transits, and any knowledge about its physical parameters could not be extrapolated to the rest of the known Hot Jupiters. This thesis work was intended principally to search for more transiting planets, in order to establish what is common and what is peculiar in these kind of objects. Though it seems obvious, we point out that this field of investigation is strongly

governed by observations; this will be demonstrated in the following chapters.

As we saw in the previous sections, there are different proposed theories to explain the apparently "too big" size of the planet HD 209458b. Some of them would implicitly require that the newly found transiting planets should also exhibit an increased radius. This subject remained an open question until the new transiting planets were detected (even after that, it remains an open question, as we will see at the end of Chapter 5).

One important obstacle we had to overcome was to establish techniques that allow the identification of the many false positives that would arise from transiting planet surveys. These will be described in Chapter 3.

Finally, the 2004 transit of Venus provided, for the first time ever, the opportunity to test the transmission spectroscopy technique, in a object whose atmosphere is at least better known than those of the far away planets orbiting stars other than the Sun. These observations will be described in Chapter 6.